ILU PRECONDITIONED MULTI-MODEL FORMULATION FOR COMPRESSIBLE FLOWS ON 3D UNSTRUCTURED MESHES

Tao Xu[1] **, Xiao-Chuan Cai**[2] **, Marius Paraschivoiu**[1]
[1]**Dept. of Mech. and Ind. Eng., Univ. of Toronto, Toronto, Canada, M5S 3G8**
[2]**Dept. of Comp. Sci., Univ. of Colorado, Boulder, CO 80309**

Keywords: *Full potential equation, Euler equations, Inexact Newton methods, Krylov space methods, ILU preconditioner*

Abstract

A preconditioned multi-model formulation for three dimensional compressible flows is presented. The goal is to minimize the overall computational time and memory required to simulate the flow by using locally selected, more computational efficient physical models without sacrificing the global fidelity of the simulation. We review a finite volume based conservative discretization for the coupling of the full potential equation and the Euler equations. The resulting nonlinear system is solved by a pseudo-transient Newton-Krylov method. The novelty in this paper is the use of an incomplete LU factorization applied to precondition the linear system derived for the multi-model formulation at each Newton step. We present computed solutions for subsonic and transonic flows around half a NACA0012 airfoil extruded in 3D to demonstrate the feasibility of this method. Results show that the ILU preconditioner works well for the multi-model formulation.

1 Introduction

Compressible fluid flow simulations needed for aerodynamic applications can be modeled with different degrees of complexity. A simple model is the full potential equation which assumes inviscid, irrotational and isentropic flows. This model utilizes a single second-order nonlinear differential equation that is inexpensive with respect to the execution time and the memory requirement. Validity of the full potential equation is, however, restricted. The isentropic assumption of the full potential flow model leads to inaccurate physics for transonic flows with strong shocks. The next level of approximation is the Euler equations which describe the complete behavior of inviscid compressible flows. The Euler model utilizes a coupled system of five nonlinear differential equations of first order. The five field variables lead to a fivefold increase in the memory needed over the full potential, for the same mesh density. Finally, the Navier-Stokes equations include the viscous effects needed for accurate modeling of the boundary layer. These equations are not only more time consuming to solve but also require an associated mesh that is stretched and very fine in viscous regions. Nevertheless, for complex flows with separation of the boundary layer, the Navier-Stokes equations are mandatory to provide an accurate simulation. Furthermore, for high Reynolds number flows, turbulence appears and needs to be modeled.

In this work, we only consider a coupling between the Full potential equation and the Euler equations. This coupling has been demonstrated in [10] for both subsonic and transonic flows over wings. Results show that convergence is reached, the solution across the interface is smooth and the solution is improved when the full potential re-

gion includes the leading edge of the wing. The use of the full potential equation does not generate artificial entropy, contrary to the us of the Euler equations. Nevertheless, the iterative solution of the coupled nonlinear problem exhibits a slow convergence. In this work, we look for possible cures to this problem by investigating a preconditioned strategy.

The solution of the coupled flow field requires the solution of a non-linear problem in the Euclidean space R^n:

$$H(x) = 0. \tag{1}$$

To solve this system we use an inexact Newton iteration strategy [3] in which the linear system is not solved exactly. Note that, in the case of our two-equations problem, the linear system has two distinct contributions, i.e., from the full potential equation and the Euler equations. The cost of solving the linear system is crucial because it is to be solved at each Newton iteration. In this paper a technique to improve the convergence of the linear system by using a better preconditioner is developed.

The remainder of this paper is as follows. In Section 2, we review numerical approaches used to dicretized the governing equations, i.e., the full potential equation and the Euler equations. Section 3 describe the multi-model formulation. In Section 4, we compare the performance of the multi-model formulation with the classical Euler formulation by analyzing the number of nonlinear iterations.

2 Compressible flow simulation

Our interest lies in the numerical simulation of three-dimensional compressible flows. This flow can be simulated by solving the Navier-Stokes equations. However, as motivated above, the inviscid regions can also be modeled with the Euler equations or with the full potential equation for the particular case when the assumptions of irrotationality and isentropy are satisfied.

2.1 Euler and Navier-Stokes equations

Assuming that there are no external forces or heat transfer, the governing system of PDEs for compressible steady flows can be expressed in coordinate-invariant form by:

$$\begin{aligned} \nabla\cdot(\rho\mathbf{u}) &= 0, & (2)\\ \nabla\cdot(\rho\mathbf{u}\mathbf{u}+p\mathbf{I}-\bar{\bar{\tau}}) &= 0, & (3)\\ \nabla\cdot((\rho e+p)\mathbf{u}-k\nabla T-\bar{\bar{\tau}}\cdot\mathbf{u}) &= 0, & (4) \end{aligned}$$

where ρ, $\mathbf{u}$ and e represent density, three-dimensional velocity, and energy field solutions, respectively. The pressure field p is determined by an algebraic equation of state,

$$p = (\gamma-1)(e-\frac{1}{2}(u^2+v^2w^2)) \tag{5}$$

where e is the internal energy and the coefficient γ is th ratio of specific heat coefficient under constant pressure and constant volume, $\gamma = c_p/c_v$. In (3), $\bar{\bar{\tau}}$ represents the viscous shear stress tensor. In (4), T and k represent the absolute temperature and the thermal conductivity coefficient, respectively.

For inviscid fluid, the equation reduce to the Euler equations:

$$\begin{aligned} \nabla\cdot(\rho\mathbf{u}) &= 0, & (6)\\ \nabla\cdot(\rho\mathbf{u}\mathbf{u}+p\mathbf{I}) &= 0, & (7)\\ \nabla\cdot((\rho e+p)\mathbf{u}) &= 0. & (8) \end{aligned}$$

To solve the Euler and Navier-Stokes equations, we take advantage of an existing code based on an unstructured finite volume discretization of the convective fluxes [5]. The computational flow domain is divided into tetrahedra to provide maximum flexibility for tessellating complex geometries. To minimize storage, flow variables are located at the vertices of the elements. This code uses a second-order flux discretization based on the standard MUSCL (Monotonic Upwind Scheme for Conservative Laws) scheme [9].

For completeness, we now briefly describe the implicit approach used to solve the Euler equations. The Navier-Stokes equations are

treated similarly but we will now only discuss the Euler equations as only the coupling between Euler and full potential domains is addressed in this paper. To ease notations, the subscript h identifies the spatial discretized functions, and Ψ_h denotes the second-order discretization of the convective fluxes. The spatial discretization of the boundary conditions is obtained using a non-reflecting version of the flux–splitting scheme [4]. A pseudo-transient approach to reach the steady state is employed. A fully discretized scheme, which is of first order in time and of second-order in space, can be written as

$$\frac{U_h^{n+1}-U_h^n}{\Delta t_h^n}+\Psi_h(U_h^{n+1})=0, \tag{9}$$

where n is a running time step and U contains the conservative variables, i.e., $U=(\rho,\rho u,\rho v,\rho w,\rho E)^T$. The local time step size Δt_h^n is defined for each control volume τ_i^c (with characteristic size $\|\tau_i^c\|$) by

$$\Delta t_h^n=\|\tau_i^c\|\frac{\mathrm{CFL}}{C_{\tau_i^c}+\|\mathbf{U}_{\tau_i^c}\|_2}, \tag{10}$$

where CFL is a preselected positive number, $C_{\tau_i^c}$ is the sound speed and $\mathbf{U}_{\tau_i^c}$ is the velocity vector. Increasing the time step by increasing the CFL inversely proportional to the residual norm is recommended. This approach is used here; the CFL at every time step is calculated as

$$\mathrm{CFL}^{n+1}=\mathrm{CFL}^n\frac{\|\Psi_h(U^{n-1}\|)}{\|\Psi_h(U^n)\|}. \tag{11}$$

We use an inexact Newton method to solve the non-linear problem (9). Given an initial solution U^0, the solution is updated at each step $n+1$ by

$$U^{n+1}=U^n+\lambda^{n+1}\delta U^{n+1} \tag{12}$$

where δU^{n+1} is an inexact solution to the linear system of equations

$$\left(\frac{\|\tau_i^c\|}{\Delta t_h^n}+\frac{\partial\Psi_h^{(1st)}(U_h^n)}{\partial U_h}\right)\delta U^{n+1}=-\Psi_h^{(2nd)}(U_h^n). \tag{13}$$

Note that the accuracy of the numerical solution is determined by how the term $\Psi_h^{(2nd)}(U_h^{n+1})$ on the right-hand side of (13) is discretized in space. However, the *cost* is mostly determined by how the left–hand side of (13) is constructed and solved. The advantage of this technique is that we can solve a first order problem but still obtain a second-order spatial accuracy by using a first order Jacobian evaluated from analytic formula with a second-order residual.

2.2 Full potential equation

To start we present the full potential equation, the spatial discretization and the implicit method. We also discuss the upwind procedure required for transonic flows.

2.2.1 Governing equations

Let $\Omega\subset\Re^3$ be the computational flow domain and Γ its boundary. For compressible inviscid and irrotational flows, there exists a potential variable Φ satisfying the full potential equation

$$\frac{\partial\rho(\Phi)}{\partial t}+\nabla\cdot G(\Phi)=0, \tag{14}$$

where $G(\Phi)=\rho\nabla\Phi$ and

$$\nabla\Phi=(u,v,w)^T. \tag{15}$$

Here, u,v, and w represent the three components of velocity. Also, note that the full potential variable, Φ, is a scalar.

By appealing the isentropic flow assumption we can write the density ρ as a nonlinear function of the potential, such as

$$\rho(\Phi)=\rho_\infty\left(1+\frac{\gamma-1}{2}M_\infty^2\left(1-\frac{||\nabla\Phi||_2^2}{q_\infty^2}-\frac{\partial\Phi}{\partial t}\right)\right)^{1/(\gamma-1)}, \tag{16}$$

where M_∞, q_∞, and ρ_∞ are the free–stream Mach number, the magnitude of the free–stream velocity and the free–stream density, respectively. $\gamma=1.4$ is the ratio of specific heat. This equation is a nonlinear second order partial differential equation which is very fast to solve numerically relative to the Euler equations. In this paper, only the steady state solution is studied. We next introduce the spatial discretization.

2.2.2 *Spatial discretization*

Using a finite volume approach, the integral form of the full potential equation for the control volume τ_i^c is simply

$$\int_{\tau_i^c} \nabla \cdot G(\Phi) \mathrm{d}A = 0. \tag{17}$$

Note that the union of τ_i^c covers the whole domain Ω, i.e., $\overline{\Omega} = \bigcup \overline{\tau_i^c}$. The triangulation is accomplished by dividing the domain into tetrahedral elements, $\tau_{i,j}$. This triangulation is the most common in the aerospace industry [11] allowing for easy triangulations of complex geometries and for adaptive mesh refinements. It is also the same triangulation of the Euler solve utilized in this study and therefore allowing easy solution transfer between the two solvers. The potential variable is stored at the vertices. An illustration, in two space dimensions, is presented in Figure 1. By using this triangulation, the space of the potential solution is taken to be piecewise linear continuous functions determined by the vertex values Φ_i.

For the control volume τ_i^c associated with the dual mesh, we can write the discrete form of (17) as

$$\begin{aligned} \int_{\tau_i^c} \nabla(\rho \nabla \Phi) dA &= \int_{\partial \tau_i^c} \rho \nabla \Phi \cdot \mathbf{n} \, dS \qquad (18) \\ &= \sum_{\tau_{i,j}} \rho_{i,j} (\nabla \Phi)_{i,j} \cdot \mathbf{S}_{i,j}^c, \end{aligned}$$

where $\tau_{i,j}$ is the "triangulation" associated with the control volume τ_i^c and $\mathbf{S}_{i,j}^c = \int_{\partial \tau_i^c \cap \tau_{i,j}} \mathbf{n} dA$. Here $\mathbf{n}$ is the unit outward normal vector of the face associated with the control volume τ_i^c in the element $\tau_{i,j}$. Note that $\rho_{i,j}$, the discrete density, is a function of $(\nabla \Phi)_{i,j}$ which is constant for each element $\tau_{i,j}$.

2.2.3 *Upwinding*

For transonic flows, upwinding is required; therefore, the density is modified to add artificial compressibility prior to the flux calculation. For simplicity we describe our upwinding method for two space dimensions. Following [8, 12], we write

$$\tilde{\rho} = \rho - \mu \mathbf{v} \cdot \nabla_{-} \rho, \tag{19}$$

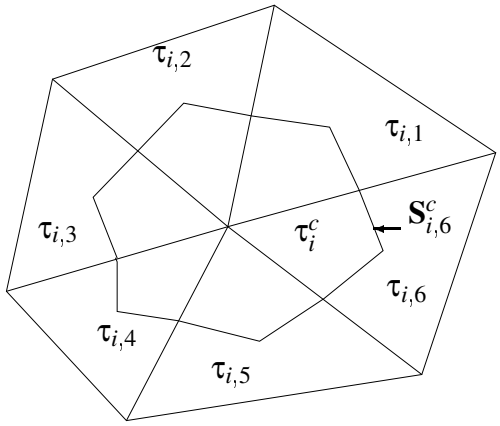

Fig. 1 Two space dimensions representation of the control volume.

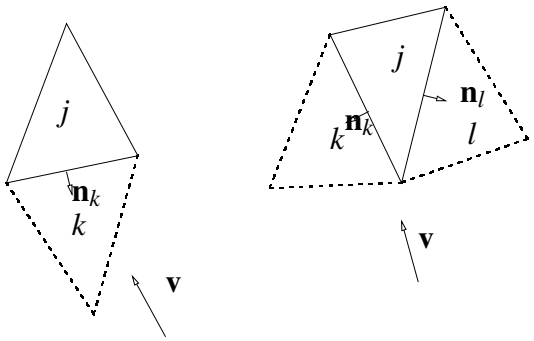

Fig. 2 Upwind configurations.

where $\mathbf{v}$ is the normalized element velocity and $\nabla_{-}\rho$ is an upwind difference. In two space dimensions there are two cases to consider. Either the mass flux enters on one side (Fig. 2.2.3 a) or the mass flux enters through two sides (Fig. 2.2.3 b). It follows that the density for each different case becomes

$$\tilde{\rho_j} = \rho_j + \mu \mathbf{v}\cdot\mathbf{n_k}(\rho_\mathbf{j} - \rho_\mathbf{k}) \quad (20)$$

$$\tilde{\rho_j} = \rho_j + \mu \mathbf{v}\cdot\mathbf{n_k}(\rho_\mathbf{j} - \rho_\mathbf{k}) + \mu \mathbf{v}\cdot\mathbf{n_l}(\rho_\mathbf{j} - \rho_\mathbf{l}). \quad (21)$$

The switching function, μ, is defined for each element as

$$\mu = \nu_o \max\{0, 1 - M_c^2/M^2\}, \quad (22)$$

where M is the element Mach number, M_c is a pre–selected cutoff Mach number chosen to introduce dissipation in the transonic regime. The parameter ν_o is used to increase the amount of dissipation in the supersonic elements. Parameters M_c and ν_o are selected by hand; M_c is just smaller than 1 and ν_o is usually set between 1 and 3. Additional viscosity is added by taking the switching function in each element to be the maximum value of all its immediate neighbors. We refer the reader to [1, 6] for more details.

2.2.4 Implicit approach

To solve (17) we introduce a pseudo–time step. Hence, we rewrite (17) as

$$\frac{d}{dt}\int_{\tau_i^c} \Phi dA + \int_{\tau_i^c} \nabla\cdot G(\Phi) dA = 0. \quad (23)$$

The semi-discrete form of (23) becomes

$$\left(\frac{\|\tau_i^c\|}{\Delta t_h^n} + \frac{\partial(\Upsilon_h(\Phi^n))}{\partial\Phi}\right)\left(\Phi_h^{n+1} - \Phi_h^n\right) = -\Upsilon_h(\Phi^n), \quad (24)$$

where Υ_h is the discrete mass flux. In this approach we require the computation of the Jacobian matrix $\partial\Upsilon_i(\Phi_i^n)/\partial\Phi$. A finite difference approximation of this Jacobian is introduced. For each pair of indices i, j we define

$$\frac{\partial(\Upsilon_i(\Phi))}{\partial\Phi_j} \approx \frac{\Upsilon_i(\Phi + \delta\Phi_j) - \Upsilon_i(\Phi)}{\delta\Phi_j}. \quad (25)$$

This first order accurate approach is chosen because a first order Jacobian is sufficient in the inexact Newton method. The resulting matrix is sparse, with contributions from the neighbors of node i only. Therefore, we do not consider this matrix to be computationally very expensive. In fact, if no upwinding is needed the calculation of the Jacobian is only about five times more expensive than calculating the mass flux .

The local time step size Δt_h^n is defined for each control volume τ_i^c (with characteristic size $\|\tau_i^c\|$) by

$$\Delta t_h^n = \|\tau_i^c\| \frac{\mathrm{CFL}}{C_{\tau_i^c} + \|\mathbf{U}_{\tau_i^c}\|_2}. \quad (26)$$

The approach to increase the CFL inversely proportional to the residual norm, recommended for the Euler solver is also used here.

3 Coupled solver

For simplicity, we describe the coupling between the full potential and the Euler solver only.

3.1 Computational domain

The computational domain, Ω, is split into two subdomains, Ω_E and Ω_Φ, wherein the Euler equations and the full potential equation are solved, respectively. We denote by Γ_I the interface between Ω_E and Ω_Φ, as shown in Figure 3.

The formulation presented for the full potential is similar to the unsteady Euler formulation for finite volumes. In fact, we can define W as the *simulation variable*, which represents either the Euler variables, U, or the full potential variable, Φ. We assume that W is the solution of the equation

$$\frac{\partial W}{\partial t} + \nabla\cdot P(W) = 0, \quad (27)$$

where the flux function P is called the *model function* that equals to either F or G, the Euler or full potential fluxes respectively.

Consider the interface between the full potential domain and the Euler domain presented in Figure 3. This interface is located between tetrahedra, therefore, the control volume associated

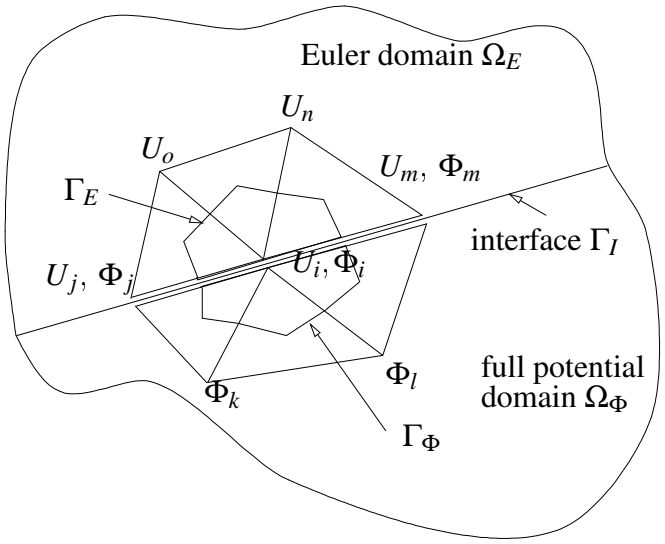

Fig. 3 Overlapping interface of the Euler and the full potential domains.

with a node on this interface is shared between both the full potential domain and the Euler domain. This control volume is considered as part of the overlapping region. Conservation laws for the Euler equations as well as the conservation laws for the full potential equation are forced on this control volume.

First, we describe discretization of the conservation laws associated with the Euler equations, i.e., the conservation of mass, momentum and energy. The fluxes across the surface of the control volume that lies in the Euler domain (Ω_E) can be readily calculated. However, we require to convert the potential variable to the Euler variable to calculate the fluxes across the surface that lies in the potential domain (Ω_Φ). To this end we use the potential to Euler variable transfer function (found in [2]) to calculate, at vertices k and l, the momentum and the energy. Note that, the density and the velocity, $\nabla\Phi$, are constant in the elements laying in the full potential domain. The value of the density and velocity in elements surrounding a vertex is averaged and used at that vertex.

Second, only the conservation of mass for an overlapping control volume is required for the full potential solver. To be more precise the conservation of mass is written as

$$\int_{\Gamma_E} \rho V \cdot \mathbf{n}_E dS + \int_{\Gamma_\Phi} \rho \nabla\Phi \cdot \mathbf{n}_\Phi dS = 0, \quad (28)$$

where ρV is the first component of the Euler flux vector. Note that in this approach we have over determined the conservations laws. Indeed, the same control volume will satisfy the conservation of mass for both the Euler equations and for the full potential equation.

3.2 Algorithmic framework

A Newton-Krylov approach is used to obtain a steady state solution of our coupled equations. The system of nonlinear equations is of the form $H(W) = 0$. A solution of the nonlinear system is sought by using an inexact Newton method. Linearization with respect to W^{n+1} yields

$$H(W^{n+1}) = H(W^n) + \frac{\partial H}{\partial W}\Delta W = 0. \quad (29)$$

Introducing J_n as the Jacobian of H with respect to W^n, we obtain

$$J_n \Delta W^n = -H(W^n). \quad (30)$$

We solve the above linear problem using a preconditioned GMRES method such that

$$\|B^{-1}(J_n \Delta W^n + H(W^n)\|_2 \leq \varepsilon \|H(W^n)\|_2, \quad (31)$$

where $\varepsilon > 0$ is the linear tolerance and the operator B^{-1} preconditiones the action of J_n.

3.3 Explicit Jacobian

For a full potential-Euler coupled solver we write

$$J_n = \frac{D}{\Delta t} + \frac{\partial \Psi(U)}{\partial U} + \frac{\partial \Psi(U)}{\partial \Phi} + \frac{\partial \Upsilon(\Phi)}{\partial U} + \frac{\partial \Upsilon(\Phi)}{\partial \Phi}, \quad (32)$$

where D is the diagonal matrix of cell volumes and Δt is the time step. We have discussed in Section 2.2.4 how to approximate $\partial\Upsilon(\Phi)/\partial\Phi$. In addition, the term $\partial\Psi(U)/\partial U$ is obtained from a classical approximation [7]. Note that $\Psi(U)$ and

$\Upsilon(\Phi)$ exist only in their respective domains and that the resulting Jacobian matrix is of the form:

$$\begin{bmatrix} \frac{\partial \Psi(U)}{\partial U} & \frac{\partial \Psi(U)}{\partial \Phi} \\ \frac{\partial \Upsilon(\Phi)}{\partial U} & \frac{\partial \Upsilon(\Phi)}{\partial \Phi} \end{bmatrix}. \tag{33}$$

The calculation of $\partial\Psi(U)/\partial\Phi$ is somewhat less standard. As before, we use a finite–difference approximation to calculate this term in the Jacobian. Our approximation becomes

$$\frac{\partial \Psi_i(U)}{\partial \Phi_j} \approx \frac{\Psi_i(U+\delta\Phi_j) - \Psi_i(U)}{\delta\Phi_j}. \tag{34}$$

Here again, we transfer $\delta\Phi$ to δU using the above described procedure to calculate the Euler fluxes, Ψ. Similarly, the following approximation is used

$$\frac{\partial(\Upsilon_j(\Phi))}{\partial U_i} \approx \frac{\Upsilon_j(\Phi+\delta U_i) - \Upsilon_j(\Phi)}{\delta U_i}. \tag{35}$$

The calculation of $\Upsilon_{i,j}$ is performed by modifying the value of node i with δU_i. Subsequently, the resulting mass flux is added to Υ_j, associated with τ_j^{Φ}.

We have omited on purpose the description of the upwinding for the full potential solver because it is not needed in our approach as we restrict the full potential domain to subsonic regions. Recall that in the Euler domain, the upwinding is intrinsic to the Roe's scheme.

3.4 ILU preconditioner

The incomplete LU factorization technique (ILU) is used to construct the preconditioner. An ILU(0) is a Gaussian elimination procedure in which fill-ins, i.e., locations originally occupied by zero values, are dropped. A more accurate factorization, where up to level k fill-ins are kept, are denoted by ILU(k).

The principal new ingredient in this implicit scheme is the calculation and investigation of the ILU preconditiones for Jacobian J_n on a multi-domain. The use of this preconditioner solves the slow convergence problem reported in [10].

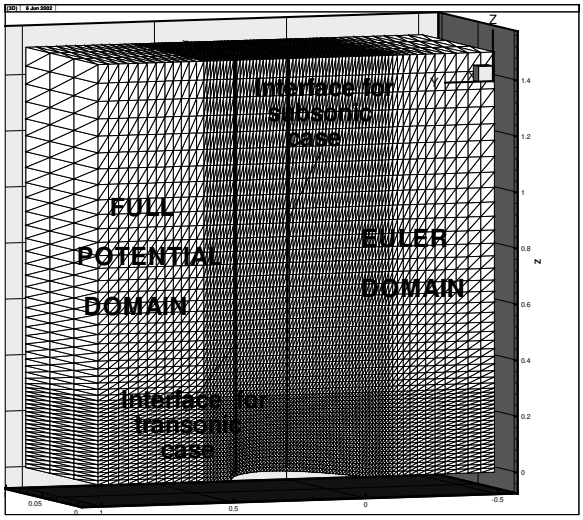

Fig. 4 Computational mesh and partition for the domain.

4 Numerical results

In this section we test our scheme for a two-dimensional flow over a NACA0012 airfoil in a three-dimensional computational domain. Only half of the geometry is required for this symmetric flow. The computational domain is such that Ω is a rectangle domain of size $0.1 \times 1.5 \times 1.5$, where an upper surface of a NACA0012 is located on the bottom face as in Figure 4. The grid used here has 25,410 nodes. The boundary conditions of this problem are as follows: on the top, left and right boundaries we impose farfield conditions; on the side and the bottom we impose the nonpenetration condition for symmetry and on the airfoil we impose the solid wall condition.

4.1 Subsonic flow

We investigate a subsonic flow around the NACA0012 wing at $M_\infty = 0.5$. The domain partitioning of this mesh into the Euler domain and the full potential domain is shown in Figure 4: the right domain is the Euler domain and the left is the full potential domain, both of which contain the same 12,810 nodes. The Mach number iso-contours for the Euler and the full potential models are shown in Figure 5 and in Figure 6, respectively. The Mach number contours for the coupled model are presented in Figure 7. Note

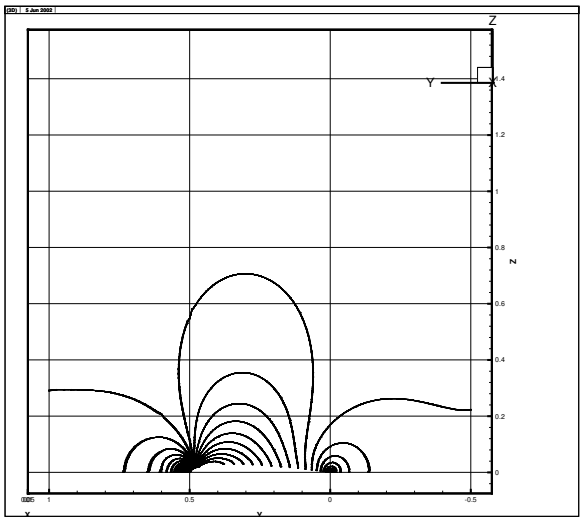

Fig. 5 Mach number contours of the full potential model solution at $M_\infty = 0.5$.

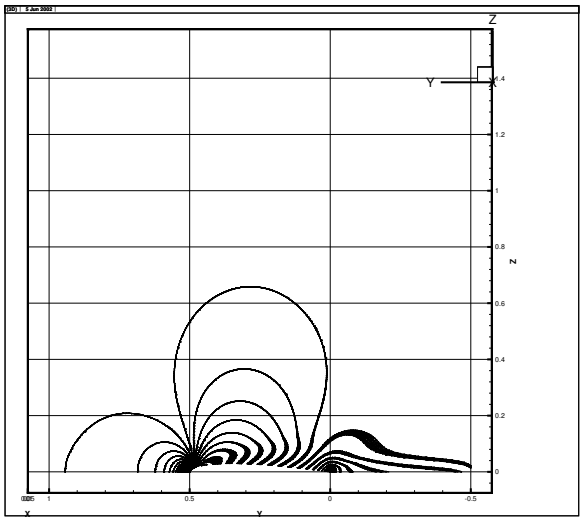

Fig. 6 Mach number contours of the Euler model solution at $M_\infty = 0.5$.

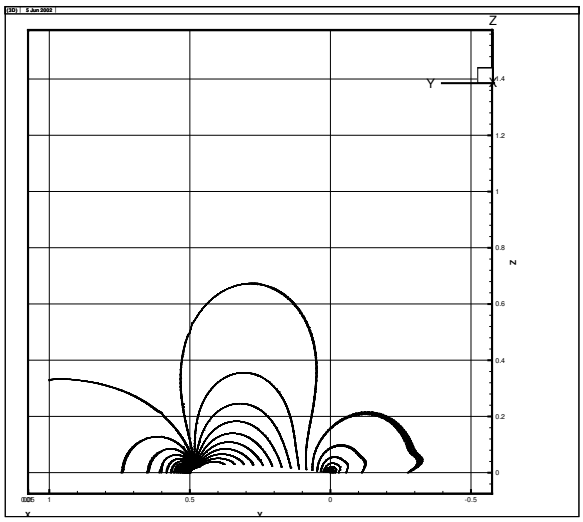

Fig. 7 Mach number contours for the solution of the coupled model at $M_\infty = 0.5$.

the smooth transition of the iso-contours between the Euler and full potential domains. Comparing the solution in Figure 5 and 7, we can say that the solution of the coupled model is better than the Euler and almost the same as the full potential models. Clearly, for subsonic flows, the full potential solution is more accurate because the flow obeys the full potential assumption. For a coarse mesh, the Euler model generates artificial entropy at the leading edge which significantly decreases the accuracy of the solution. In our case, the mesh is indeed coarse and the artificial entropy can be noticed near the airfoil surface and in the wake, Figure 6. In the coupled model, the leading edge is part of the full potential domain, therefore minimizing the artificial entropy generated by the Euler model.

Figure 8 compares the nonlinear iterations of the Euler model, the coupled model and the coupled model with ILU(0) and ILU(1). Clearly we can see that the incomplete LU preconditioner dramatically speeds up the convergence of the coupled model. Comparing higher level ILU with ILU(0), higher level fill-in does not really improve the speed of convergence. Note that the full potential solver is very faster. The solution is obtained in 32 iterations with a residual less than 10^{-8}. However, when this solver is coupled

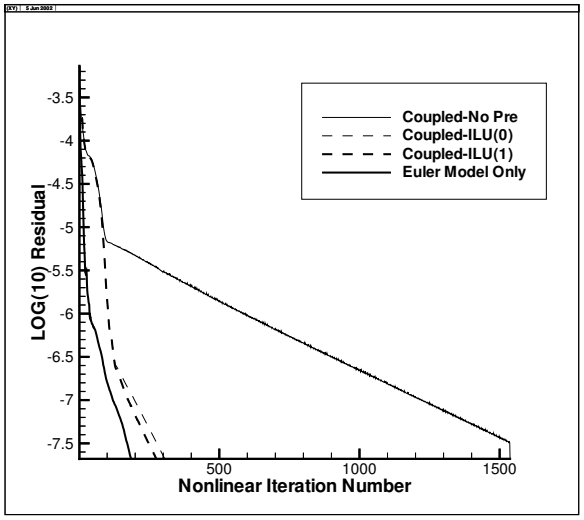

Fig. 8 Convergence iteration history for subsonic flow around the NACA0012 wing.

with the Euler solver, the number of iterations increased to 1537. This is far more than the 211 pseudo time iterations needed in the Euler model. With the ILU(0) or the ILU(1) applied to precondition the flux coupled Jacobian, the nonlinear iteration decreased to 355 and 326, respectively.

4.2 Transonic flow

To illustrate the multi-model formulation for transonic problems, we investigate a flow around the NACA0012 wing at $M_\infty = 0.8$. The domain is partitioned along a constant y plane located at $y = 0.5$. The Euler domain (right) and the full potential domain (left) each contain 19,110 and 6510 nodes, respectively. In Figures 9 and 10, we show the Mach number iso-contours for values of 0.3 to 1.26 with an increment of 0.03, for the Euler solution and the coupled solution, respectively. Note the smooth transition of the iso-contours between the Euler and full potential domains in the latter.

The performance of the coupled nonlinear solver, in terms of the number of nonlinear iterations, is presented in Figure 11. The Euler solution is obtained in 184 iterations with a residual less than 10^{-8}. The Euler solver uses a maximum number of 30 linear iteration in the GMRES solver. A convergence study revealed that the same number of nonlinear iterations was

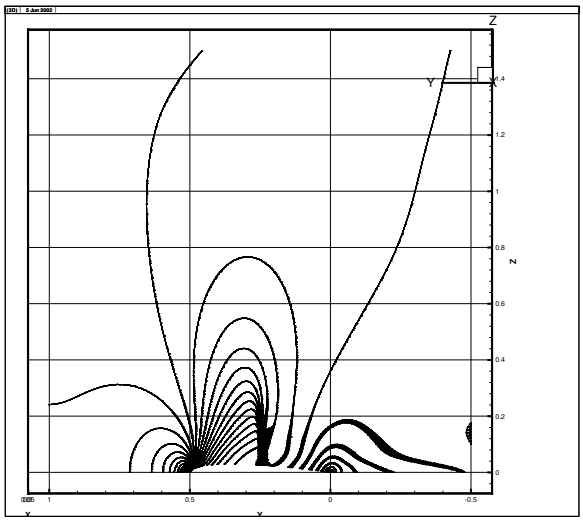

Fig. 9 Mach number contours for the Euler model solution at $M_\infty = 0.8$.

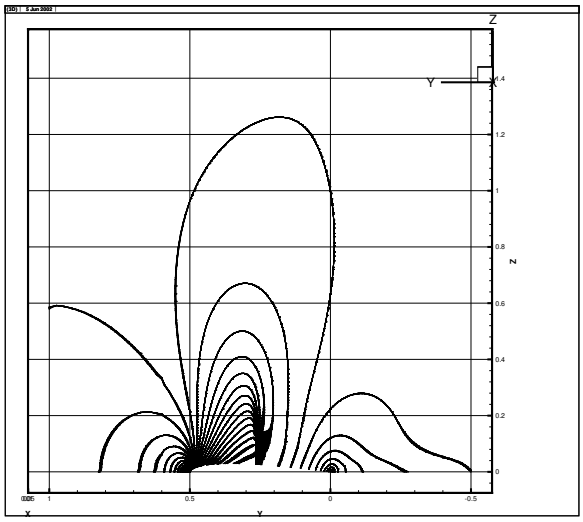

Fig. 10 Mach number contours for the coupled model solution at $M_\infty = 0.8$.

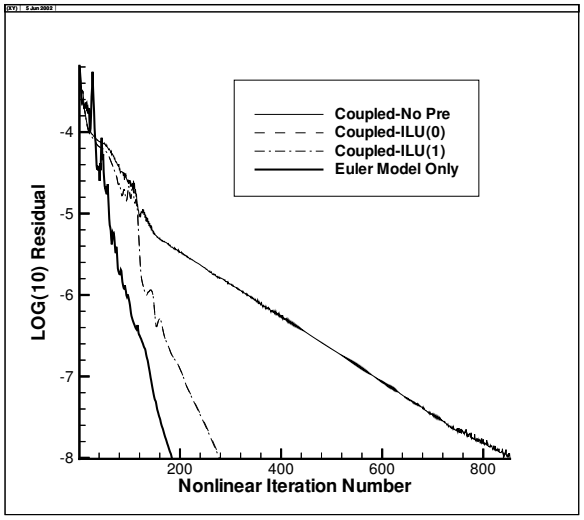

Fig. 11 Convergence iteration history for transonic flow around the NACA0012 wing.

required with or without ILU preconditioners. This can be explained by the use of the inexact Newton method. However, when the coupled solver is used without preconditioners, the number of iterations increased to 853. The ILU(0) or ILU(1) preconditioners accelerate convergence. The number of iterations decreased to 280 for ILU(0) and 278 for ILU(1).

References

[1] Cai X.-C, Gropp W. D, Keyes D. E, Melvin R. G, and Young D. P. Parallel Newton–Krylov–Schwarz algorithms for the transonic full potential equation. *SIAM J. Sci. Comput.*, Vol. 19, pp 246–265, 1998.

[2] Cai X.-C, Paraschivoiu M, and Sarkis M. An explicit multi–model compressible flow formulation based on the full potential equation and the Euler equations. *Proc Proc. of the* 11^{th} *Intl. Conference on Domain Decomposition Methods*, pp 157–174, 1999.

[3] Dembo R, Eisenstat S, and Steihaug T. Inexact newton methods. *SIAM J Numerical Analysis*, Vol. 19, pp 400–4008, 1982.

[4] Farhat C and Lanteri S. Simulation of compressible viscous flows on a variety of MPPs: Computational algorithms for unstructured dynamic meshes and performance results. *Comput. Meths. Appl. Mech. Engrg.*, Vol. 119, pp 35–60, 1994.

[5] Farhat C, Lesoinne M, and Maman N. Mixed explicit/implicit time integration of coupled aeroelastic problems: three-field formulation, geometric conservation and distributed solution. *Int. J. Numer. Methods Fluids*, Vol. 21, pp 807–835, 1995.

[6] Habashi W. G and Hafez M. M. Finite element solutions of transonic flow problems. *AIAA J.*, Vol. 20, pp 1368–1375, 1982.

[7] Hirsch C. *Numerical Computation of Internal and External Flows*. John Wiley & Sons, New York, 1990.

[8] Holst T. L and Ballhaus W. F. Fast, conservative schemes for the full potential equation applied to transonic flows. *AIAA J.*, Vol. 17, pp 145–152, 1979.

[9] Leer B. V. Towards the ultimate conservative difference scheme. V. A second order sequel to Godunov's method. *J. Comput. Phys.*, Vol. 32, pp 361–370, 1979.

[10] Paraschivoiu M, Cai X.-C, Sarkis M, Young D. P, and Keyes D. An implicit multi–model compressible flow formulation based on the full potential equation and the Euler equations. *AIAA Paper 99-0784*, 1999.

[11] Peraire J and Morgan K. Unstructured mesh generation including directional refinement for aerodynamic flow simulation. *Finite Elements in Analysis and Design*, Vol. 25, pp 343–356, 1997.

[12] Young D. P, Mervin R. G, Bieterman M. B, Johnson F. T, Samant S. S, and Bussoletti J. E. A locally refined rectangular grid finite element methods: Application to computational fluid dynamics and computational physics. *J. Comput. Phys.*, Vol. 92, pp 1–66, 1991.